applied sciences

MDPI

Technical Note

Nonlinear Vibration Response of a Rectangular Tube with a Flexible End and Non-Rigid Acoustic Boundaries

Yiu-Yin Lee

Department of Civil and Architectural Engineering, City University of Hong Kong, Kowloon Tong, Kowloon, Hong Kong; bcraylee@cityu.edu.hk

Academic Editor: César M. A. Vasques
Received: 13 September 2016; Accepted: 5 December 2016; Published: 10 December 2016

Abstract: This paper addresses the analysis for the nonlinear vibration response of a rectangular tube with a flexible end and non-rigid acoustic boundaries. The structural–acoustic modal formulations are developed from the Duffing differential equation and wave equation, which represent the large-amplitude structural vibration of a flexible panel coupled with a cavity. This problem considers both non-rigid acoustic boundary and structural cubic nonlinearity. The multi-level residue harmonic balance method is employed for solving the nonlinear coupled differential equations developed in the problem. The results obtained from the proposed method and numerical method are generally in good agreement. The effects of excitation magnitude, tube length, and phase shift parameter, etc., are examined.

Keywords: nonlinear plate vibration; structural acoustics; harmonic balance method

1. Introduction

In the well-known acoustic text book [1], an investigation of resonating tube/pipe accounts for the properties of a mechanical driver, which is driven by external excitation (see Figure 1). The driver has its own mechanical impedance. Thus, the system considers the coupling between a linear spring-mass and an internal cavity with rigid acoustic boundaries. Similar to other structural–acoustic problems, the aforementioned problem does not include the structural nonlinearity and non-rigid acoustic boundary.

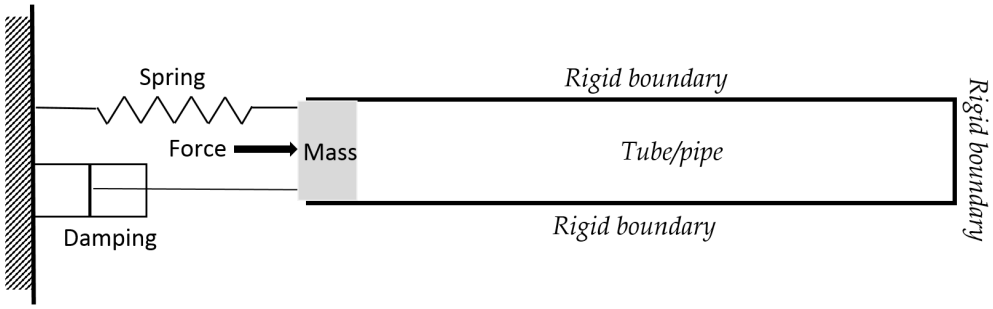

Figure 1. The linear structural–acoustic model in [1].

In practice, there are many engineering problems with structural acoustics, a few examples being: (1) the sound absorption of a panel absorber backed by an air cavity; (2) the vibration response of an aircraft cabin which is a "tube-like" structure enclosing a cavity; and (3) the noise within a rectangular ventilation duct that is formed by thin metal sheets. In these examples, the structures are usually made of thin metal panels and are easily excited to vibrate nonlinearly, and the boundaries of the cavities are

not perfectly rigid or fully open. In fact, there have been many research works about linear structural acoustics (e.g., [2–4]) or nonlinear vibrations (e.g., [5–12]). However, there are limited works about nonlinear structural–acoustic problems with non-rigid acoustic boundary conditions. This study is a further work of the aforementioned linear structural–acoustic problem in [1]. Thus, this paper would focus on structural nonlinearity and non-rigid acoustic boundary. Moreover, the multi-level residue harmonic balance method, which was developed by Leung and Guo [13] in 2011, and then modified by Hansan et al. [14] in 2013, is employed to solve the nonlinear differential equations, which represent the large-amplitude structural vibration of a flexible panel coupled with a cavity. Table 1 shows the numbers of algebraic equations generated in the multi-level residue harmonic balance method and the classical harmonic method for a cubic nonlinear undamped beam problem. When compared with the classical harmonic balance method, this harmonic balance method requires less computational effort because it requires solving one nonlinear algebraic equation and one set of linear algebraic equations for obtaining each higher-level solution. The solutions from the proposed method are verified by those from the classical harmonic balance method. Parametric studies are performed, and the effects of structural nonlinearity and acoustic boundary condition on the nonlinear vibration responses are investigated in detail.

Table 1. Numbers of equations for the cubic nonlinear undamped beam problem.

Solution Method	Zero Level (1 Harmonic Term)		1st Level (2 Harmonic Terms)		2nd Level (3 Harmonic Terms)	
	No. of nonlinear algebraic equations	No. of linear algebraic equations	No. of nonlinear algebraic equations	No. of linear algebraic equations	No. of nonlinear algebraic equations	No. of linear algebraic equations
Proposed harmonic balance method	1	0	1	2	1	3
Classical harmonic balance method	1	0	2	0	3	0

2. Theory

Figure 2 shows the general concept of a structural–acoustic model, in which the structural part is in contact with a finite cavity by physical boundaries. The enclosed volume would induce the acoustic resonant behavior, which is normally modeled using the well-known wave equation [1,2,15–17]. This wave equation has been used in numerous applied science/engineering problems for the past few decades. The structural part in the model usually is a plate or a shell, which is subject to an external force and coupled with the internal acoustic pressure within the cavity. The structural vibration directly affects the magnitude of the acoustic pressure acting on the structure. This is so-called structural–acoustic interaction. In the past, many researchers just focused on particular linear/nonlinear plate modellings (e.g., [5–12,18]) or linear structural–acoustic problems with perfectly rigid acoustic boundaries. In this paper, the focuses include the nonlinear structural–acoustic interaction and non-rigid acoustic boundary. Figure 3 shows the problem considered in this study. The acoustic pressure within the rectangular tube is obtained from the homogeneous wave equation.

$$\nabla^2 P^h - \frac{1}{C_a^2}\frac{\partial^2 P^h}{\partial t^2} = 0 \tag{1}$$

where P^h is the h-th harmonic component of the acoustic pressure within the cavity; Ca is the speed of sound.

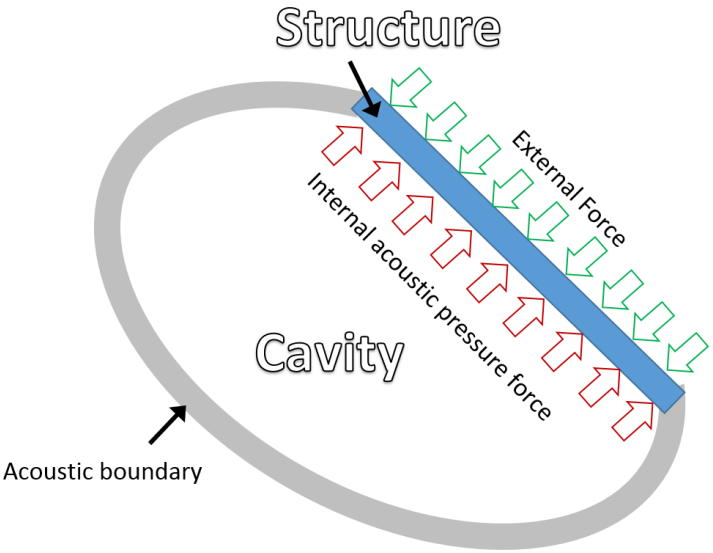

Figure 2. General concept of a structural–acoustic model.

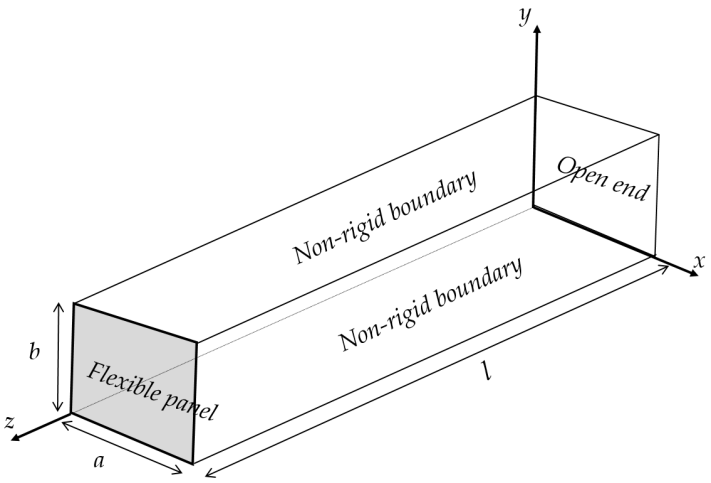

Figure 3. Schematic diagram of a rectangular tube with a flexible end and non-rigid acoustic boundaries.

In Figure 4, the boundary conditions of the perfectly rigid and fully open cases at $x = 0$ and a; $y = 0$ and b are given by

$$\frac{\partial P^h}{\partial x} = \frac{\partial P^h}{\partial y} = 0, \text{ for perfectly rigid} \tag{2a}$$

$$P^h = 0, \text{ for fully open} \tag{2b}$$

According to Equations (2a) and (2b), the acoustic pressure mode shapes of the perfectly rigid and fully open cases are given by

$$\varphi_{uv}(x,y) = \cos\left(\frac{u\pi}{a}x\right)\cos\left(\frac{v\pi}{b}y\right) \tag{3a}$$

$$\varphi_{uv}(x,y) = \sin\left(\frac{(u+1)\pi}{a}x\right)\sin\left(\frac{(v+1)\pi}{b}y\right) \tag{3b}$$

where $\varphi_{uv}(x,y)$ is the (u,v) acoustic mode, a and b are the cross-sectional dimensions of the duct, and u and v are the acoustic mode numbers.

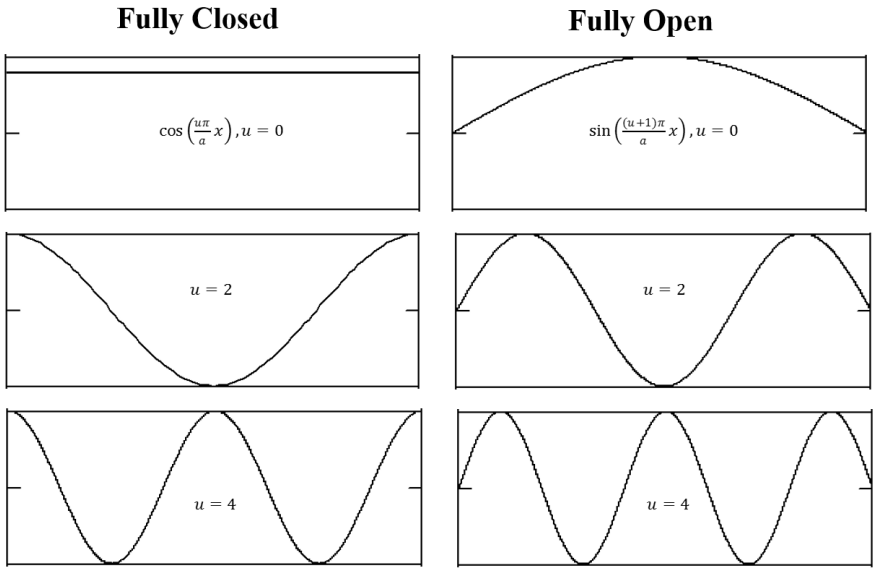

Figure 4. Acoustic mode shapes of the fully open and fully closed cavity boundaries.

Hence, the acoustic pressure mode shape of non-rigid case is defined by

$$\varphi_{uv}(x,y) = \cos\left(\frac{(u+\eta)\pi}{a}x - \eta\frac{\pi}{2}\right)\cos\left(\frac{(v+\eta)\pi}{b}y - \eta\frac{\pi}{2}\right) \tag{4}$$

where $\eta = \frac{\theta}{90}$; θ is the phase shift parameter. If η is set as zero in Equation (4), then the acoustic mode shapes become those in the perfectly rigid case.

The boundary conditions at $z = l$ and 0 are given by

$$\frac{\partial P^h}{\partial z} = -\rho_a \frac{\partial^2 w_c^h}{\partial t^2} \text{ at } z = l \tag{5a}$$

$$P^1 = P_o \sin(\omega t) \text{ at } z = 0, \text{ for } h = 1 \tag{5b}$$

$$P^h = 0 \text{ at } z = 0, \text{ for } h \neq 1 \tag{5c}$$

where l is the duct length; ρ_a = air density; ω = excitation frequency. Note that the external sound pressure at $z = 0$ is simple harmonic excitation (i.e. no higher harmonic components). P_0 = excitation magnitude, $\gamma \times P_{ref}$; γ is the dimensionless parameter; P_{ref} is the reference pressure level, 10^2 N/m^2. $w_l^h(x,y,t)$ = the h^{th} harmonic component of the nonlinear panel displacement at $z = l$.

$$w_l^h(x,y,t) = A_{h,\sin}(t)\phi_{mn}(x,y) \tag{6}$$

where $\phi_{mn}(x,y) = \sin\left(\frac{m\pi x}{a}\right)\sin\left(\frac{n\pi y}{b}\right)$ = the (m,n) panel mode (it is simply supported). $A_{h,\sin}(t) = A_h \sin(h\omega t)$; A_h is the panel vibration amplitude. The total response of the panel is equal to the summation of all harmonic components and given by

$$w_l(x,y,t) = \sum_{h=1,3,5\ldots}^{H} w_l^h(x,y,t) = \sum_{h=1,3,5\ldots}^{H} A_{h,\sin}(t)\phi_{mn}(x,y) \tag{7}$$

where $w_c(x,y,t)$ is the displacement response of the panel at $z = l$. H = the number of harmonic terms. Then, the multi-level residue harmonic balance method is adopted for solving the differential equations and obtaining the unknown panel displacement responses. For simplicity, only the zero, 1st

and 2nd level solution procedures (or three harmonic components are considered) are shown here. According to the multi-level residue harmonic balance solution form proposed in [14,19],

$$A(t) = \varepsilon^0 A0(t) + \varepsilon^1 A1(t) + \varepsilon^2\, A2(t) \tag{8}$$

where ε is an embedding parameter. Any terms associated with ε^0, ε^1, ε^2 represent those terms considered in the zero, 1st and 2nd level solution procedures respectively. Then, the zero, 1st and 2nd level solutions, $A0(t)$, $A1(t)$ and $A2(t)$, are given by

$$A0(t) = A0_1 \sin(\omega t) \tag{9a}$$

$$A1(t) = A1_1 \sin(\omega t) + A1_3 \sin(3\omega t) \tag{9b}$$

$$A2(t) = A2_1 \sin(\omega t) + A2_3 \sin(3\omega t) + A2_5 \sin(5\omega t) \tag{9c}$$

The 1st, 2nd and 3rd harmonic components of the total displacement amplitude, A_1, A_2 and A_3, are given by

$$A_1 = A0_1 + A1_1 + A2_1 \tag{10a}$$

$$A_3 = A1_3 + A2_3 \tag{10b}$$

$$A_5 = A2_5 \tag{10c}$$

Then, the solution form of the acoustic pressure in Equation (1) is given by [1,2,15,16,19]

$$P^h(x,y,z,t) = \sum_u^U \sum_v^V \left[L_{uv}^h \sinh\left(\mu_{uv}^h z\right) + N_{uv}^h \cosh\left(\mu_{uv}^h z\right) \right] \varphi_{uv}(x,y) \sin(h\omega t) \tag{11}$$

where $\mu_{uv}^h = \sqrt{\left(\frac{(u+\eta)\pi}{a}\right)^2 + \left(\frac{(v+\eta)\pi}{b}\right)^2 - \left(\frac{h\omega}{C_a}\right)^2}$; L_{uv}^h and N_{uv}^h are coefficients that depend on the boundary conditions at $z = 0$ and $z = l$; U and V are the numbers of acoustic modes used.

The unknown coefficients L_{uv}^h and N_{uv}^h can be obtained by applying the boundary condition at $z = 0$ and $z = l$ in Equations (5a)–(5c) to Equation (11). They are given by for $h = 1$, $N_{uv}^1 = P_o \frac{\alpha_{uv}^0}{\alpha_{uv}^{uv}}$ and $L_{uv}^1 = \rho_a \frac{\omega^2 A_1}{\mu_{uv}^1 \cosh(\mu_{uv}^1 l)} \frac{\alpha_{uv}^{mn}}{\alpha_{uv}^{uv}} - P_o \frac{\alpha_{uv}^0}{\alpha_{uv}^{uv}} \tanh(\mu_{uv}^1 l)$; for $h \neq 1$, $N_{uv}^h = 0$ and $L_{uv}^h = \frac{\rho_a (h\omega)^2}{\mu_{uv}^h} \frac{1}{\alpha_{uv}^{uv}} \left(\frac{\alpha_{uv}^{mn} A_h}{\cosh\left(\mu_{uv}^h l\right)} \right)$; $\alpha_{uv}^o = \int_0^b \int_0^a \varphi_{uv} dxdy$; $\alpha_{uv}^{uv} = \int_0^b \int_0^a \varphi_{uv} \varphi_{uv} dxdy$; $\alpha_{uv}^{mn} = \int_0^b \int_0^a \varphi_{uv} \phi_{mn} dxdy$; $\alpha_{mn}^{mn} = \int_0^b \int_0^a \phi_{mn} \phi_{mn} dxdy$.

Once L_{uv}^h and N_{uv}^h are obtained, the modal pressure force magnitude at $z = l$ can be found using Equation (11)

$$\overline{P}_l^1 = K_A^1 A_1 + K_o^1 P_o, \text{ for } h = 1 \tag{12a}$$

$$\overline{P}_l^h = K_A^h A_h, \text{ for } h \neq 1 \tag{12b}$$

where $K_A^1 = \sum_u^U \sum_v^V \frac{\rho_a \omega^2}{\mu_{uv}^1} \frac{(\alpha_{uv}^{mn})^2}{\alpha_{uv}^{uv} \alpha_{mn}^{mn}} \tanh(\mu_{uv}^1 l)$; $K_o^1 = \sum_u^U \sum_v^V \frac{\alpha_{uv}^{mn} \alpha_{uv}^o}{\alpha_{mn}^{mn} \alpha_{uv}^{uv}} \frac{1}{\cosh(\mu_{uv}^1 l)}$.

In this study, the nonlinear free vibration formulation of panel adopted in [16] is employed.

$$\rho_l \frac{d^2 A}{dt^2} + \rho_l \omega_l^2 A + \beta_l A^3 = 0 \tag{13}$$

where ρ_l and ω_l are the surface density and linear resonant frequency of the panel; β_l represents the nonlinear stiffness coefficient due to the large-amplitude vibration.

$$\beta_l = \frac{E\tau}{4(1-v^2)} \left(\frac{m\pi}{a}\right)^4 \left[\left(1 + \left(\frac{n}{m} r\right)^4\right) \left(\frac{3}{4} - \frac{v^2}{4}\right) + v \left(\frac{n}{m} r\right)^2 \right] \tag{14}$$

where $r = a/b$ is the aspect ratio; ν is the Poisson's ratio. E is the Young's modulus. τ is the panel thickness.

By putting the acoustic force terms developed from Equations (12a) and (12b) into Equation (13), the governing equation for the nonlinear forced vibrations is given by

$$\rho_l \frac{d^2A}{dt^2} + \rho_l \omega_l^2 A + \beta_l A^3 + \sum_{h=1,3,5...}^{H} K_A^h A_h \sin(h\omega t) = K_o^1 P_o \sin(\omega t) \tag{15}$$

Substitute Equation (9) into Equation (15) and consider those terms associated with ε^0. Then consider the harmonic balance of $\sin(\omega t)$. The zero-level equation without the damping term is given by

$$\left(K_A^1 + \Pi(\omega)\right) A0_1 + \frac{3}{4}\beta_l A0_1^3 = K_o^1 P_o \tag{16}$$

where $\Pi(\omega) = \rho_l\left(-\omega^2 + \omega_l^2\right)$; The unbalanced residual in the zero-level procedure is $\Delta_{A0} = -\frac{1}{4}\beta_l A0_1^3 \sin(3\omega t)$.

According to Equation (16), the damped vibration amplitude is given in the following form

$$A0_1 = \frac{K_o^1 P_o}{\left(K_A^1 + \pi(\omega)\right) + \frac{3}{4}\beta_l |A0_1|^2} \tag{17}$$

where $\Pi(\omega) = \rho_l\left(-\omega^2 + \omega_l^2\right) + j\left(C_a \rho_a \omega + \xi \omega \omega_p\right)$; $j = \sqrt{-1}$; ξ is the internal material damping coefficient; ω_p is the nonlinear resonant peak frequency; "$C_a \rho_a \omega$" represents the radiation damping term [1,20].

Again, substitute Equation (9) into Equation (15) and consider those terms associated with ε^1 to obtain the following 1st level equation

$$\left(K_A^1 + \pi(\omega)\right) A1_1 \sin(\omega t) + \left(K_A^3 + \pi(3\omega)\right) A1_3 \sin(3\omega t) + 3\beta_l (A0)^2 A1 + \Delta_{A0} = L_1 \tag{18}$$

where L_1 represents the summation of the 1st level terms and the unbalanced residual in the zero level. Δ_{A0} is the residual in the zero level.

Then, consider the harmonic balances of $\sin(\omega t)$ and $\sin(3\omega t)$ for Equation (18)

$$\int_0^{2\pi} L_1 sin(\omega t) dt = 0 \tag{19a}$$

$$\int_0^{2\pi} L_1 sin(3\omega t) dt = 0 \tag{19b}$$

Hence, $A1_1$ and $A1_3$ can be found by solving Equations (19a) and (19b).

Similarly, substitute Equation (9) into Equation (15) and consider those terms associated with ε^2 to obtain the following 2nd level equation

$$\begin{gathered}(K_A^1 + \pi(\omega)) A2_1 \sin(\omega t) + (K_A^3 + \pi(3\omega)) A2_3 \sin(3\omega t) + (K_A^5 + \pi(5\omega)) A2_5 \sin(5\omega t) \\ +3\beta_c A0 (A1)^2 + 3\beta_l A2 (A0)^2 + \Delta_{A1} = L_2\end{gathered} \tag{20}$$

where L_2 represents the summation of the 2nd level terms and the unbalanced residual in the 1st level. Δ_{A1} is the residual in the zero level.

Then, consider the harmonic balances of $\sin(\omega t)$, $\sin(3\omega t)$ and $\sin(5\omega t)$ for Equation (20)

$$\int_0^{2\pi} L_2 \sin(\omega t) dt = 0 \tag{21a}$$

$$\int_0^{2\pi} L_2 \sin(3\omega t) dt = 0 \tag{21b}$$

$$\int_0^{2\pi} L_2 \sin(5\omega t) dt = 0 \tag{21c}$$

Hence, $A2_1$, $A2_3$ and $A2_5$ can be found by solving Equations (21a)–(21c).

3. Results and Discussion

In this section, the material properties in the numerical cases are as follows: Young's modulus = 7.1×10^{10} N/m^2, Poisson's ratio = 0.3, and mass density = 2700 kg/m^3; panel dimensions = 0.4 m × 0.4 m × 2 m; damping ratio ξ = 0.02. Tables 2–4 show the convergence studies of normalized panel vibration amplitude for various excitation magnitudes and frequencies. The nine acoustic mode solutions, three structural mode solutions, and 2nd level solutions are normalized as one hundred. The acoustic boundaries are rigid (i.e., $\theta = 0$). The zero, 1st and 2nd level solutions contain 1, 2 and 3 harmonic components, respectively (i.e., $\sin(\omega t)$, $\sin(3\omega t)$, and $\sin(5\omega t)$). It is shown that the 1st level 4 acoustic mode and two structural mode approach is good enough for convergent and accurate vibration amplitude solution.

Table 2. Acoustic mode convergence study (1st level solution, number of structural modes = 2, $l = 5a$, $\gamma = 4$).

ω/ω_c	No. of Acoustic Modes		
	1	**4**	**9**
1.8	99.83	100.00	100 [1]
2.8	99.09	99.97	100 [1]
4.8	99.97	100.24	100 [1]

[1] The amplitudes are normalized as 100.

Table 3. Structural mode convergence study (1st level solution, number of acoustic modes = 4, $l = 5a$, $\gamma = 4$).

ω/ω_c	No. of Structural Modes		
	1	**2**	**3**
1.8	99.20	100.00	100 [1]
2.8	98.77	100.00	100 [1]
4.8	70.28	99.97	100 [1]

[1] The amplitudes are normalized as 100.

Table 4. Harmonic term convergence study (number of structural modes = 2, number of acoustic modes = 4, $l = 5a$, $\gamma = 4$).

ω/ω_c	No. of Harmonic Terms		
	1 (Zero Level)	**2 (1st Level)**	**3 (2nd Level)**
1.8	103.60	100.66	100 [1]
2.8	100.17	100.00	100 [1]
4.8	99.83	100.00	100 [1]

[1] The amplitudes are normalized as 100.

Figures 5–7 present the comparisons between the vibration amplitudes obtained from the present harmonic balance method and numerical method used in [6]. The results obtained from the two methods are generally in good agreement. Note that the numerical method is unable to generate the unstable solutions. For fair comparisons, the unstable solutions from the harmonic balance methods are not generated. In fact, the classical harmonic balance method can be coupled with the asymptotic

numerical method, which enables the capture of unstable solutions (e.g., [21–23]). According to [14], the solutions from the proposed method come from the cubic algebraic equations transformed from the Duffing differential equations representing the nonlinear panel vibration. The unstable solutions occur when the cubic algebraic equations have three real solutions. Generally, the unstable solution is in between the nonlinear and nearly linear solutions. It is slightly lower than the real nonlinear solution around the peak frequency and slightly higher than the nearly linear solution when the excitation frequency is far from the peak frequency.

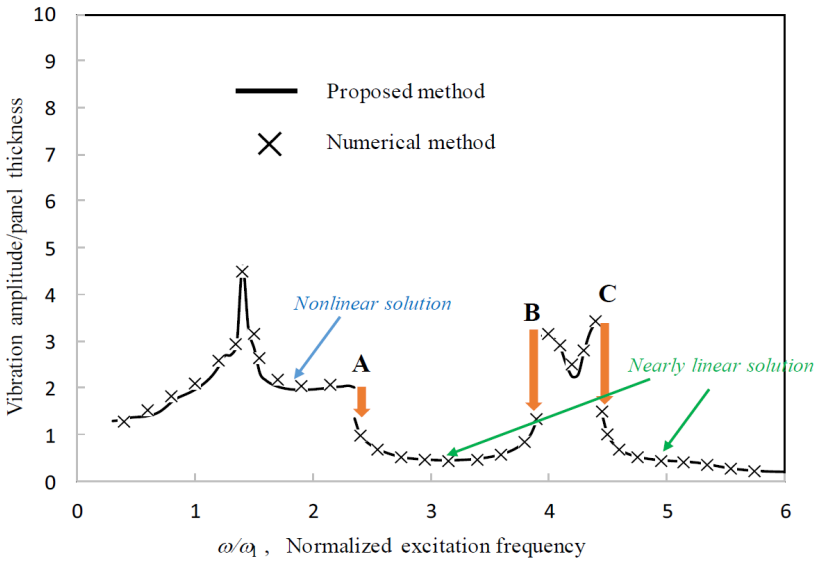

Figure 5. Comparison between the solutions obtained from the proposed method and numerical integration method [6] (number of structural modes = 2, number of acoustic modes = 4, $l = 5a$, $\gamma = 2$, $\theta = 0$; the orange arrows represent the "jump phenomenon"; "**A**", "**B**", and "**C**" represent the particular points on the solution curve).

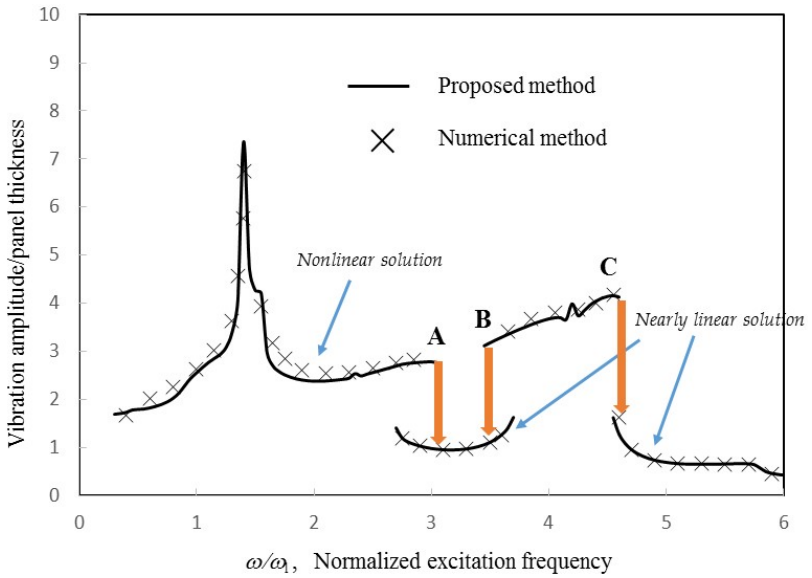

Figure 6. Comparison between the solutions obtained from the proposed method and numerical integration method [6] (number of structural modes = 2, number of acoustic modes = 4, $l = 5a$, $\gamma = 4$, $\theta = 0$; the orange arrows represent the "jump phenomenon"; "**A**", "**B**", and "**C**" represent the particular points on the solution curve).

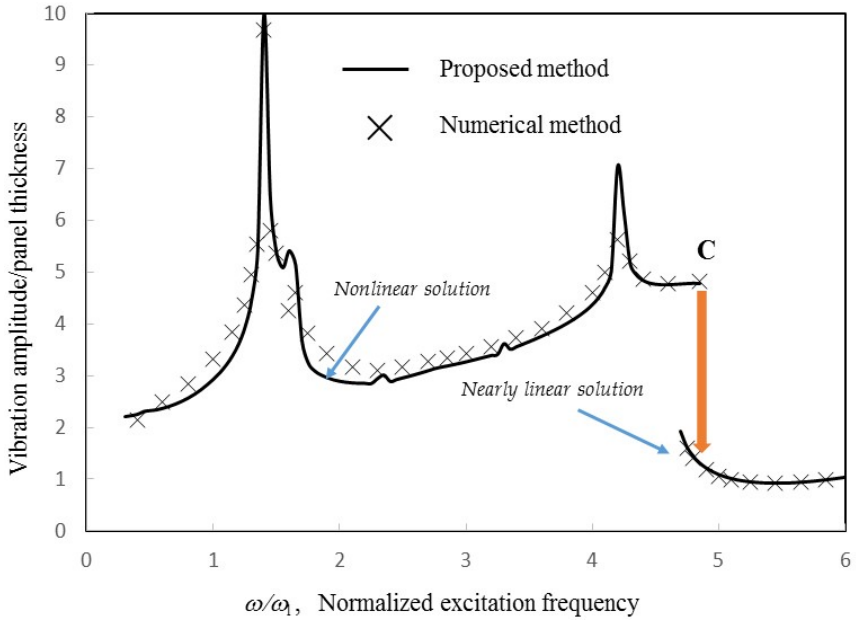

Figure 7. Comparison between the solutions obtained from the proposed method and numerical integration method [6] (number of structural modes = 2, number of acoustic modes = 4, $l = 5a$, $\gamma = 8$, $\theta = 0$; the orange arrow represents the "jump phenomenon"; "**C**" represents the particular point on the solution curve).

Relatively, the agreement in Figure 5 is the best because of smaller nonlinearity. In Figures 6 and 7, some deviations are observed around the major peak values. Note that there are some minor peaks around $\omega/\omega_l = 2.3$ and 3.4 in Figure 7. In these three cases, the first acoustic resonances occur around $\omega/\omega_l = 1.4$. In the case of $\gamma = 2$, the well-known jump phenomena, which are due to the first structural resonance and higher acoustic resonances, occurs around $\omega/\omega_l = 2.3$, 3.9 and 4.5 (see Points A, B and C). The nonlinear solution line discontinues there. Generally, the nearly linear solution lines are much lower than the nonlinear solution lines. In the cases of $\gamma = 4$ and 8, the jump phenomena due to the first structural resonance and higher acoustic resonances occur at the higher frequencies. Unlike the trough on the solution line in the case of $\gamma = 2$, a small peak and a large peak occur on the nonlinear solution lines of $\gamma = 4$ and 8 around $\omega/\omega_l = 4.2$, respectively. Besides, Points A and B in the case of $\gamma = 4$ are very close. There are no Points A and B in the case of $\gamma = 8$ (i.e., no discontinuous portion). In Figure 7, due to the large excitation level, the vibration responses are highly nonlinear. The nonlinear solution lines further extend so that Points A and B are joined and the linear solution line disappears. In this case, there is only one real solution obtained from the cubic algebraic equation transformed from the Duffing differential equations representing the nonlinear panel vibration. In the practical structural design of a similar structural–acoustic system, the disappearance of the linear solution (or small-amplitude solution), which is replaced by the nonlinear solution (or large-amplitude solution), implies that a stronger structural design is needed to overcome the larger vibration amplitude.

Figures 8–10 show the vibration amplitude plotted against the excitation frequency for various tube lengths. The first peak value due to the acoustic resonance and first jump-down frequency increase with the tube length, while the first peak frequency and the first trough frequency decrease with the tube length. In the case of $l = 10a$, the tube length is the longest among the three cases. Thus, the second peak occurs around $\omega/\omega_l = 2.1$, which is lower than the first jump-down frequency, and there are more acoustic resonant peaks on the solution line. In the case of $l = 3a$, the tube length is the shortest among the three cases. The trough occurs out of the frequency range (i.e. $\omega/\omega_l > 6$).

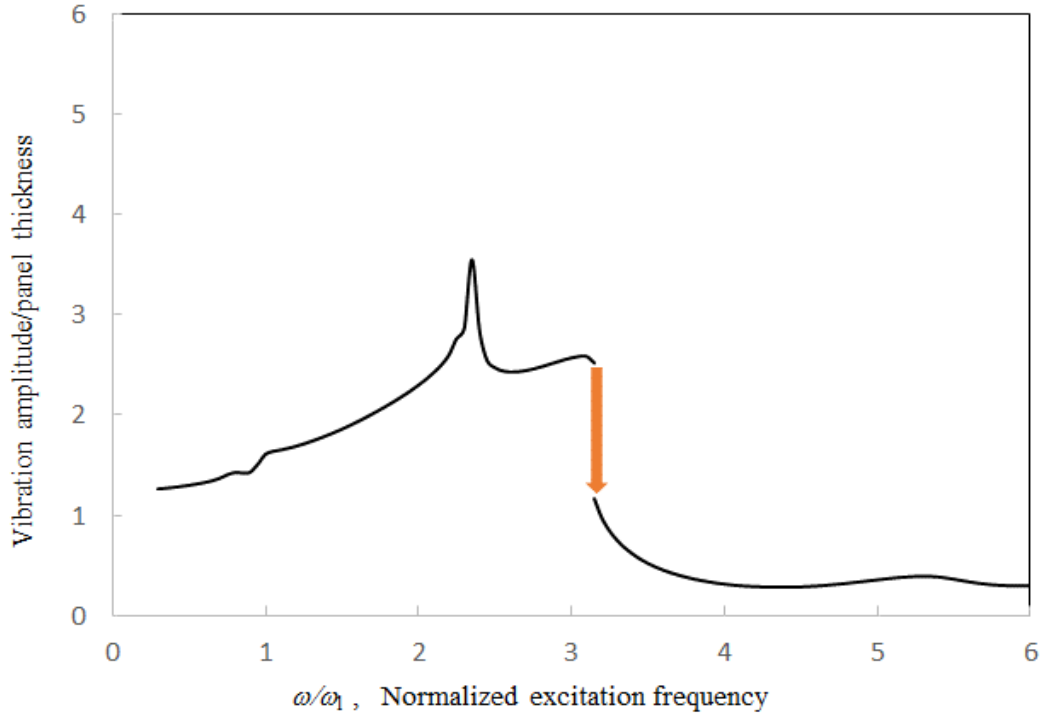

Figure 8. Vibration amplitude ratio versus normalized excitation frequency for various duct lengths (number of structural modes = 2, number of acoustic modes = 4, $\gamma = 2$, $\theta = 0$, $l = 3a$; the orange arrow represents the "jump phenomenon").

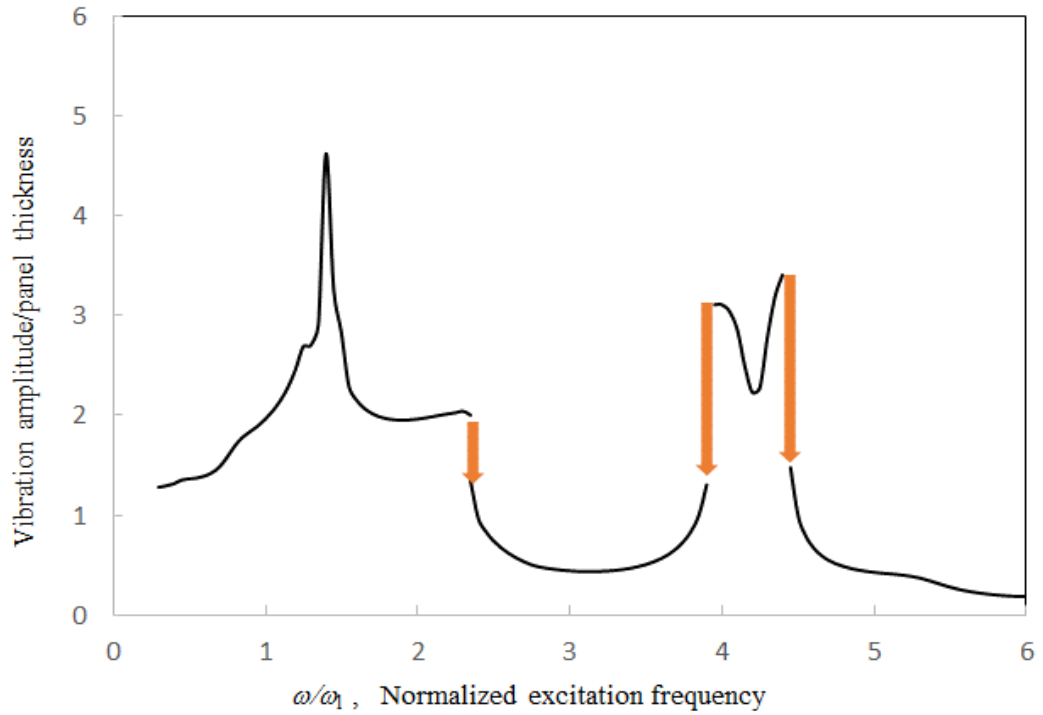

Figure 9. Vibration amplitude ratio versus normalized excitation frequency for various duct lengths (number of structural modes = 2, number of acoustic modes = 4, $\gamma = 2$, $\theta = 0$, $l = 5a$; the orange arrows represent the "jump phenomenon").

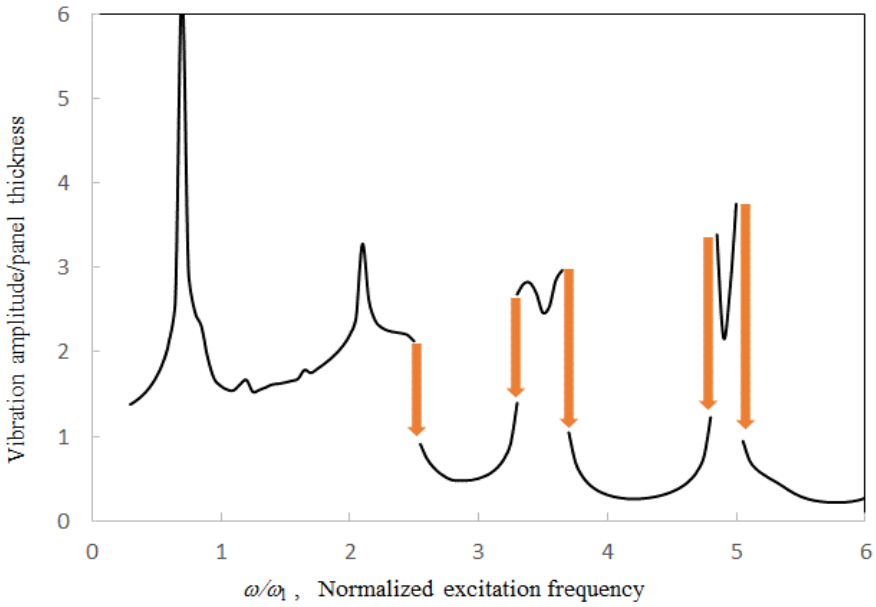

Figure 10. Vibration amplitude ratio versus normalized excitation frequency for various duct lengths (number of structural modes = 2, number of acoustic modes = 4, γ = 2, θ = 0, l = 10a; the orange arrows represent the "jump phenomenon").

Figures 11–13 show the vibration amplitude plotted against the excitation frequency for various phase shift parameters. The first peak frequency due to the acoustic resonance, the first jump-down frequency, and the trough frequency increase with the phase shift parameter, while the first peak value decreases with the tube length. In the cases of θ = 5 and 10, it is implied that the tube boundaries are not perfectly rigid and the corresponding air particle velocities are non-zero. It is noted that the first peak is quite small, marginally detectable when the phase shift is only 8 degrees.

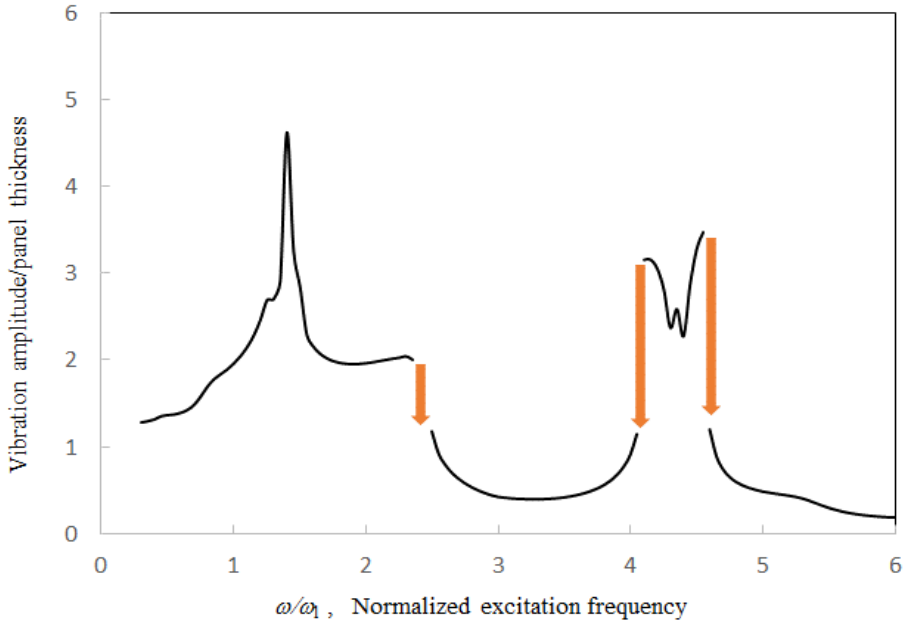

Figure 11. Vibration amplitude ratio versus normalized excitation frequency for various acoustic boundary conditions (number of structural modes = 2, number of acoustic modes = 4, γ = 2, θ = 0, l = 5a; the orange arrows represent the "jump phenomenon").

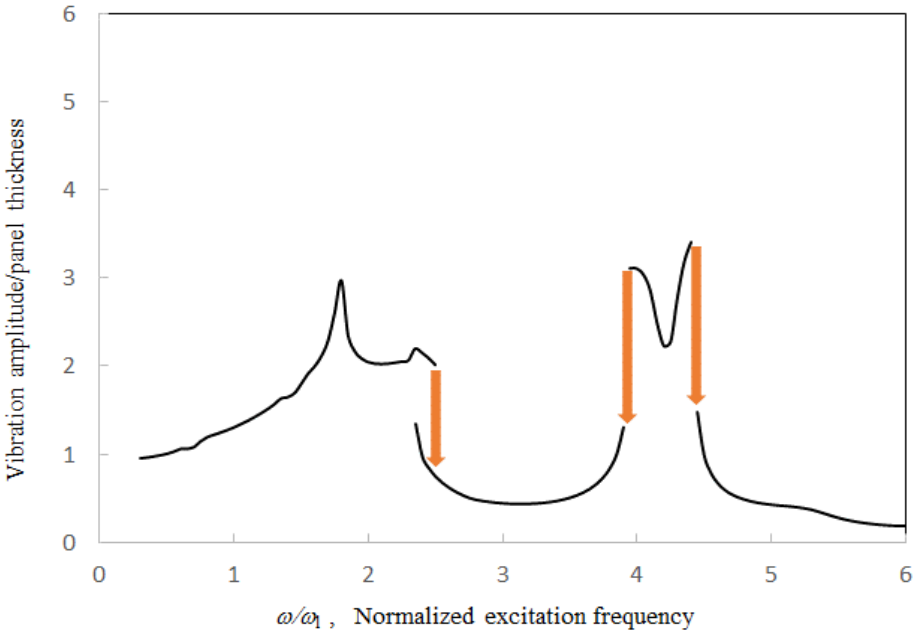

Figure 12. Vibration amplitude ratio versus normalized excitation frequency for various acoustic boundary conditions (number of structural modes = 2, number of acoustic modes = 4, γ = 2, θ = 5, $l = 5a$; the orange arrows represent the "jump phenomenon").

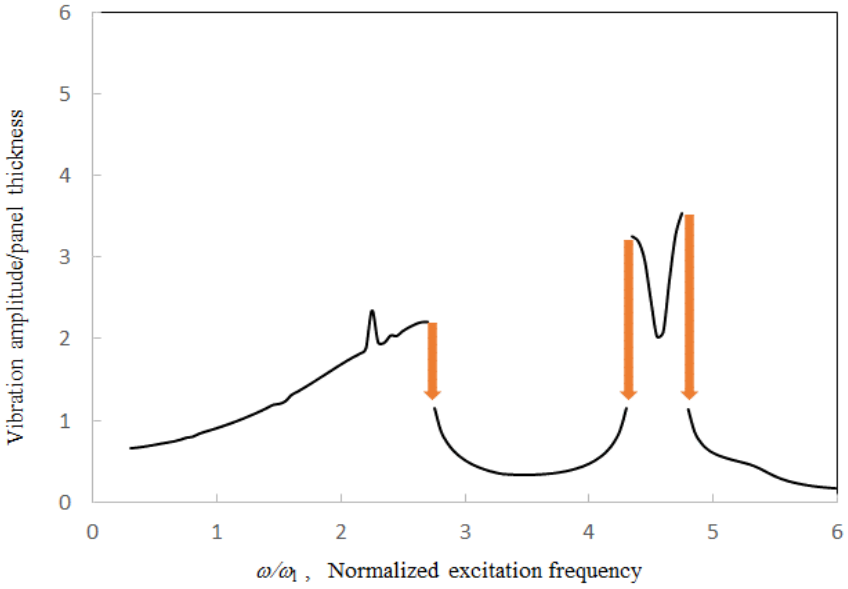

Figure 13. Vibration amplitude ratio versus normalized excitation frequency for various acoustic boundary conditions (number of structural modes = 2, number of acoustic modes = 4, γ = 2, θ = 8, $l = 5a$; the orange arrows represent the "jump phenomenon").

Moreover, the phase shift does not significantly affect the higher acoustic resonances. Figure 14 shows the vibration amplitudes of the tubes filled with air and CO_2 plotted against the corresponding excitation frequency. The density of CO_2 and the corresponding sound speed are about 50% higher than those in the case of air. There is a big difference between the two cases. In the case of CO_2, the first peak is much smaller and the jump phenomenon disappears. The peaks due to higher acoustic resonances are out of the frequency range. In the practical structural design of a similar structural–acoustic system, the disappearance of the nonlinear solution (or large-amplitude solution), which is replaced by the

linear solution (or small-amplitude solution), implies that a smaller amount of structural material is needed.

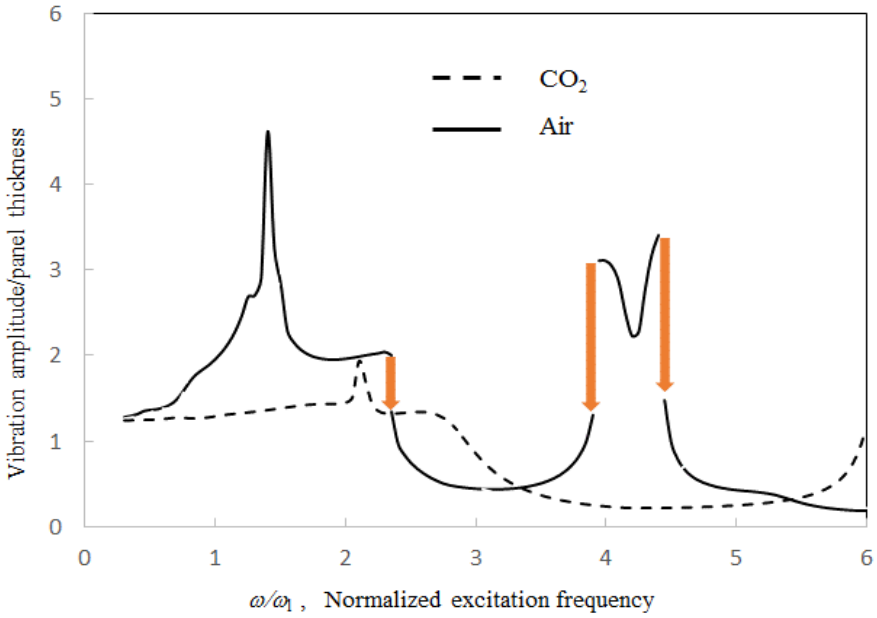

Figure 14. Vibration amplitude ratio versus normalized excitation frequency for the cases of air and CO_2 (number of structural modes = 2, number of acoustic modes = 4, $l = 5a$, $\gamma = 2$, $\theta = 0$; the orange arrows represent the "jump phenomenon").

4. Conclusions

This paper has presented the analysis for the nonlinear vibration response of a rectangular tube with a flexible end and non-rigid acoustic boundaries. The structural–acoustic modal formulations have been developed from the partial differential equations, which represent the large-amplitude structural vibration of a flexible panel coupled with a cavity. The results obtained from the multi-level residue harmonic balance method and numerical method are generally in good agreement. The effects of excitation magnitude, tube length, and phase shift parameter, etc., are investigated. It can be concluded from the results that: (1) if the excitation level is very high, there is no linear solution at the medium frequency range, and a nonlinear solution occurs at that frequency range; (2) if the tube length is longer, more vibration peaks due to the acoustic resonances appear within the particular frequency range; (3) these peak values are also very sensitive to the phase shift parameter. As an example, the first peak is marginally detectable when the phase shift is only 8 degrees; (4) if the tube is filled with CO_2, of which the density and corresponding sound speed are about 50% higher than those of air, the vibration peaks become very small or disappear within the particular frequency range.

Acknowledgments: The work described in this paper was fully supported by the CityU SRG [project No. 7004701].

Conflicts of Interest: The author declares no conflict of interest.

References

1. Kinsler, L.E.; Frey, A.R.; Coppens, A.B.; Sanders, J.V. *Fundamentals of Acoustics*, 4th ed.; John Wiley & Sons Inc.: Hoboken, NJ, USA, 2000.
2. Pretlove, A.J. Free vibrations of a rectangular panel backed by a closed rectangular cavity. *J. Sound Vib.* **1965**, *2*, 197–209. [CrossRef]
3. Oldham, D.J.; Hillarby, S.N. The acoustical performance of small close fitting enclosures. Part I: Theoretical models. *J. Sound Vib.* **1991**, *150*, 261–281. [CrossRef]

4. Lee, Y.Y.; Lee, E.W.M. Widening the sound absorption bandwidths of flexible micro-perforated curved absorbers using structural and acoustic resonances. *Int. J. Mech. Sci.* **2007**, *49*, 925–934. [CrossRef]
5. Younesian, D.; Sadri, M.; Esmailzadeh, E. Primary and secondary resonance analyses of clamped-clamped micro-beams. *Nonlinear Dyn.* **2014**, *76*, 1867–1884. [CrossRef]
6. Lee, Y.Y.; Su, R.K.L.; Ng, C.F.; Hui, C.K. The effect of the modal energy transfer on the sound radiation and vibration of a curved panel: Theory and experiment. *J. Sound Vib.* **2009**, *324*, 1003–1015. [CrossRef]
7. Lee, Y.Y.; Poon, W.Y.; Ng, C.F. Anti-symmetric mode vibration of a curved beam subject to autoparametric excitation. *J. Sound Vib.* **2006**, *290*, 48–64. [CrossRef]
8. Huang, J.L.; Su, R.K.L.; Lee, Y.Y.; Chen, S.H. Nonlinear vibration of a curved beam under uniform base harmonic excitation with quadratic and cubic nonlinearities. *J. Sound Vib.* **2011**, *330*, 5151–5164. [CrossRef]
9. Kacem, N.; Hentz, S.; Pinto, D.; Reig, B.; Nguyen, V. Nonlinear dynamics of nanomechanical beam resonators: Improving the performance of NEMS-based sensors. *Nanotechnology* **2009**, *20*, 275501. [CrossRef] [PubMed]
10. Kacem, N.; Hentz, S. Bifurcation topology tuning of a mixed behavior in nonlinear micromechanical resonators. *Appl. Phys. Lett.* **2009**, *95*, 183104. [CrossRef]
11. Kacem, N.; Arcamone, J.; Perez-Murano, F.; Hentz, S. Dynamic range enhancement of nonlinear nanomechanical resonant cantilevers for highly sensitive NEMS gas/mass sensor applications. *J. Micromech. Microeng.* **2010**, *20*, 045023. [CrossRef]
12. Kacem, N.; Baguet, S.; Duraffourg, L.; Jourdan, G.; Dufour, R.; Hentz, S. Overcoming limitations of nanomechanical resonators with simultaneous resonances. *Appl. Phys. Lett.* **2015**, *107*, 073105. [CrossRef]
13. Leung, A.Y.T.; Guo, Z. Feed forward residue harmonic balance method for a quadratic nonlinear oscillator. *Int. J. Bifurc. Chaos* **2011**, *21*, 1783–1794. [CrossRef]
14. Hasan, A.S.M.Z.; Lee, Y.Y.; Leung, A.Y.T. The multi-level residue harmonic balance solutions of multi-mode nonlinearly vibrating beams on an elastic foundation. *J. Vib. Control* **2016**, *22*, 3218–3235. [CrossRef]
15. Lee, Y.Y.; Ng, C.F. Sound insertion loss of stiffened enclosure plates using the finite element method and the classical approach. *J. Sound Vib.* **1998**, *217*, 239–260. [CrossRef]
16. Hui, C.K.; Lee, Y.Y.; Reddy, J.N. Approximate elliptical integral solution for the large amplitude free vibration of a rectangular single mode plate backed by a multi-acoustic mode cavity. *Thin-Walled Struct.* **2011**, *49*, 1191–1194. [CrossRef]
17. Park, S.; Kim, H. Development of analytical impact force models for floor impact vibration and acoustic numerical analysis. *Appl. Sci.* **2016**. [CrossRef]
18. Luo, Z.; Zhu, Y.P.; Liu, H.P.; Wang, D.Y. Dynamic similitude design method of the distorted model on variable thickness cantilever plates. *Appl. Sci.* **2016**. [CrossRef]
19. Lee, Y.Y. The effect of leakage on the sound absorption of a nonlinear perforated panel backed by a cavity. *Int. J. Mech. Sci.* **2016**, *107*, 242–252. [CrossRef]
20. Lee, Y.Y. Multi-level residue harmonic balance method for the transmission loss of a nonlinearly vibrating perforated panel. *Int. J. Struct. Stab. Dyn.* **2016**, *16*, 1450100. [CrossRef]
21. Kacem, N.; Baguet, S.; Hentz, S.; Dufour, R. Computational and quasi-analytical models for non-linear vibrations of resonant MEMS and NEMS sensors. *Int. J. Non-linear Mech.* **2011**, *46*, 532–542. [CrossRef]
22. Souayeh, S.; Kacem, N. Computational models for large amplitude nonlinear vibrations of electrostatically actuated carbon nanotube-based mass sensors. *Sens. Actuators A* **2014**, *208*, 10–20. [CrossRef]
23. Jallouli, A.; Kacem, N.; Bourbon, G.; Le Moal, P.; Walter, V.; Lardies, J. Pull-in instability tuning in imperfect nonlinear circular microplates under electrostatic actuation. *Phys. Lett. A* **2016**, *380*, 3886–3890. [CrossRef]

© 2016 by the author; licensee MDPI, Basel, Switzerland. This article is an open access article distributed under the terms and conditions of the Creative Commons Attribution (CC-BY) license (http://creativecommons.org/licenses/by/4.0/).